sustainability

MDPI

Article

Fabrication of Bamboo-Based Activated Carbon for Low-Level CO_2 Adsorption toward Sustainable Indoor Air

Sujeong Heo [1], Wooram Kim [1], Youngmin Jo [1] and Adedeji Adebukola Adelodun [2,3,*]

[1] Department of Applied Environmental Science, Kyung Hee University, Yogin-si 17104, Gyeonggi-do, Republic of Korea; hsuuj@khu.ac.kr (S.H.); woojoa@khu.ac.kr (W.K.); ymjo@khu.ac.kr (Y.J.)
[2] Department of Chemistry, University of Copenhagen, Universitetsparken 5, DK-2100 Copenhagen, Denmark
[3] Department of Marine Science and Technology, The Federal University of Technology, P.M.B. 704, Akure 340110, Nigeria
* Correspondence: aaa@chem.ku.dk

Abstract: This study fabricated a low-cost activated carbon (AC) adsorbent from readily available bamboo trees to control indoor CO_2 levels and reduce energy costs associated with sustaining clean indoor air. Bamboo is naturally high in potassium content and has narrow fibrous channels that could enhance selective CO_2 adsorption. The prepared bamboo-based activated carbon (BAC) exhibits predominantly micropores with an average pore size of 0.17 nm and a specific surface area of 984 m^2/g. Upon amination, amine functionalities, such as pyridine, pyrrole, and quaternary N, were formed on its surface, enhancing its CO_2 adsorption capacity of 0.98 and 1.80 mmol/g for low-level (3000 ppm) and pure CO_2 flows at the ambient condition, respectively. In addition, the 0.3% CO_2/N_2 selectivity ($\alpha_{s,g}$) of the prepared sorbents revealed a superior affinity of CO_2 by BAC (8.60) over coconut shell-based adsorbents (1.16–1.38). Furthermore, amination enhanced BAC's $CO_2\alpha_{s,g}$ to 13.4. These results exhibit this sustainable approach's potential capabilities to ensure the control of indoor CO_2 levels, thereby reducing the cost associated with mechanical ventilation systems. Further research should test the new sorbent's adsorption properties (isotherm, kinetics, and thermodynamics) for real-life applicability.

Keywords: indoor air quality; sustainable adsorbent; carbon dioxide; activated carbon; surface functionality

Citation: Heo, S.; Kim, W.; Jo, Y.; Adelodun, A.A. Fabrication of Bamboo-Based Activated Carbon for Low-Level CO_2 Adsorption toward Sustainable Indoor Air. *Sustainability* **2024**, *16*, 1634. https://doi.org/10.3390/su16041634

Academic Editors: Eric P. Johnson and Shengwei Zhu

Received: 23 October 2023
Revised: 25 January 2024
Accepted: 7 February 2024
Published: 16 February 2024

1. Introduction

The ever-advancing modernization increases indoor comfort, resulting in extended human indoor residence over the years [1]. Generally, humans now spend up to 90% of their daily hours indoors, including in cars, transportation cabins, malls, etc. [2]. Most times, the unconducive outdoor weather conditions require that the indoor space be isolated. Such confined spaces render indoor air quality (IAQ) inferior to outdoors, where more pronounced convective mixing enables easier dilution of polluted air with natural and cleaner air [3]. Since most indoor air pollutants (IAPs) are usually imperceivable by humans, the physical identification, characterization, and prompt avoidance of these IAPs become cumbersome [4]. Yet, the negative impact of their presence indoors, especially on human health, demands a reliable, available, affordable, but selective method for efficient and sustainable management.

Carbon dioxide (CO_2) has been an essential indicator for IAQ Management. Not that CO_2 directly harms humans upon direct exposure, but it reduces human working efficiency by lowering mental concentration, causing drowsiness and other sick-building syndrome symptoms [5]. Exposure to high CO_2 concentrations for a long time may cause headaches or vomiting [6]. Thus, managing the concentration below a certain level is desirable through mechanical or natural ventilation. These approaches to reduce indoor

thermal discomfort and the sick-building syndrome associated with elevated CO_2 levels are often energy-intensive and unsustainable [5,7]. As the airtightness of modern buildings increases due to elevated energy costs, the CO_2 concentrations in indoor spaces usually rise above the standard value [8].

The maximum permissible CO_2 concentrations in indoor spaces is 800–1000 ppm. At various concentrations, inhaled CO_2 could induce some health effects: physiological changes at >500 ppm [1], irregular heart rates and blood pressure at >600, sick-building syndrome (SBS) symptoms, reduction in cognitive level and mental performance at >1000 ppm, especially in children [5,6], and inhibition of various metabolic, respiratory, circulatory, skeletal, and renal systems at >10,000. Acute poisoning at 2000–4000 and 1000–2700 ppm for respective 2 and $\leq$6 h exposure duration could cause inflammation and cognitive depreciation [7,8]. Some indoor CO_2 exposure limits indicate IAQ levels and, thus, have been adopted as monitoring standards for IAQ: $\leq$1000, 1000–1500, and >1500 ppm levels are generally regarded as good, moderate, and poor IAQ [9,10]. Therefore, there is an imperative need to find a sustainable control technology against the incessantly increasing indoor CO_2 levels globally.

Concerning the control methods, isolating modern indoor CO_2 concentrations from the influence of outdoor concentrations of >10% is challenging, especially those arising from various industrial, commercial, and traffic-related combustion processes [11]. Over the years, absorption into monoethanolamine (MEA) has been commonly used for high-concentration CO_2 removal from industrial emission sources [12,13]. However, due to the unsustainability of absorption (i.e., exhibiting strong chemical bonding at the MEA–CO_2 absorption interface, causing tedious and energy-intensive regeneration and reuse, enormous waste generation, and material corrosion) [14,15], it became imperative to identify a viable material and technique that circumvents the demerits earlier mentioned.

Dry-phase adsorption has sufficed as the most effective and commercialized method for low-concentration CO_2 capture of approximately 1000–3000 ppm found in multi-use indoor spaces (such as subways, buses, libraries, school classrooms, offices, and workshops) at room temperature [12,16]. Adsorption has the advantages of less energy demand, ease of regeneration and reuse, ease of handling and engineering for specific applications, and abundant starting material options for environmental applications [17,18].

Although many carbon capture materials, such as metal-organic frameworks (MOFs), zeolites, carbon nanotubes (CNTs), cellulose, silica gel, polymers, and others, have been developed, they require extreme cost or low efficiency for low-concentration CO_2 [19,20]. MOFs are arguably the most porous adsorbents in the market today. The surface area of these inorganic–organic complex materials could reach up to 15,000 $m^2 \cdot g^{-1}$ [21]. However, besides their high cost and toxicity, their selective adsorption is low, making them unsuitable for gaseous separation as much as they are efficient gas storage materials [18]. Similarly, zeolites are efficient CO_2 adsorbents. However, their affinity for moisture compromises their efficiencies for low-level CO_2 removal from indoor spaces. Specifically, coconut shell-based activated carbon (AC) is a prominent CO_2 adsorbent. However, its availability is increasingly limited due to environmental protection, natural resource conservation, and other competing applications of the palm fruit [19]. As a result, AC manufacturers are opting for more readily available stock materials for efficient ACs, such as bamboo [20,22]. Although recently developed bamboo-based ACs are applied in water purification, the adsorbent's structure is considered helpful in capturing gaseous pollutants because of the similar cellulose and lignin components to those of coconut shell, which usually results in highly developed micropores through carbonization [19,23,24]. Above all, unlike the features of coal-based or coconut-based ACs, bamboo's high potassium content would be advantageous for capturing acidic gases, such as the weak Lewis acid CO_2 [25,26]. Since CO_2 in indoor spaces is relatively low, its selective adsorption is essential, and the potassium component of bamboo would aid such separation.

This study used a lignocellulosic domestic bamboo-based AC to capture indoor-level CO_2 selectively. In addition to the intrinsic potassium in the sorbent material, basic nitrogen

functionalities were doped on the AC via amination [27]. Besides its tendency to make microporous adsorbent for indoor CO_2 removal, bamboo's high potassium content makes it an excellent and highly sustainable option for making microporous and selective CO_2 dry scrubbers.

The prepared adsorbents were examined for pure (100%) and selective (0.3%) CO_2 adsorption. Their physical properties and data were compared with those of commercial coconut-based activated carbon materials to evaluate their applicability for real-life use.

2. Experimental Method

2.1. Materials

Raw bamboo (*Phyllostachys bambusoides*) stem was acquired from a local market in Yongin-si, South Korea. The samples were cut into approximately 2 cm width and washed copiously under running tap water to remove the debris attached to the surfaces. After, it was air-dried in a clean environment. Further, to remove the sample's moisture content and desorb other gaseous substances adsorbed, we dried it in an oven at 110 °C for 24 h before storing it in an airtight desiccator until the CO_2 adsorption experiment. To compare its efficiency with prominent and commercialized CO_2 adsorbents, commercially available granular coconut-based activated carbon materials, CAC1 (GA, Kuraray, Japan) and CAC2 (Wi-Fine Tech., Chungju, Republic of Korea), were procured as controlled samples. CAC1 and CAC2 have a specific surface area of >1000 $m^2 \cdot g^{-1}$ (Table 1) and are specialized for gaseous harmful substances, such as formaldehyde and toluene, in indoor spaces.

Table 1. Properties of commercial coconut shell-based activated carbons.

Sample	Density ($g \cdot cm^{-3}$)	Specific Surface Area ($m^2 \cdot g^{-1}$)	Iodine Adsorption ($mg \cdot g^{-1}$)
CAC1 (Coconut shell-based AC from Kurary)	2.0	>1000	>900
CAC2 (Coconut shell-based AC from Wi-Fine Tech., Chungju, Republic of Korea)	2.1	>1100	>1000

2.2. Methods

2.2.1. Preparation of the Activated Cabon

Figure 1 illustrates the steps in preparing the bamboo-based activated carbon (BAC-N). First, the bamboo specimens were carbonized through thermal decomposition, and pores of various sizes and structures were formed through activation [16]. The carbonization was carried out in a quartz reactor (50 mm internal diameter and 100 mm length) for 3 h at 600 °C in an electric furnace under an inert nitrogen atmosphere, preventing the lignin and cellulose components from decomposing [28]. Approximately 200 g of the material was placed in the reactor before the furnace's temperature was ramped to the target temperature at 5 $°C \cdot min^{-1}$ and held for 6 h. Then, the reactor was allowed to cool to room temperature, and the carbonized material was retrieved.

To develop the porosity and surface area of the carbonized material, we activated the material at 800 °C for approximately 2 h under vapor at a <1.4 $mL \cdot (g_{char} \cdot h)^{-1}$ flow rate. After the AC had been formed, it was cooled to room temperature and retrieved for further processing. The AC was then ground in a mortar. It was then sieved through a 2–3 mm mesh before storing in an airtight negative-pressure desiccator at room temperature.

2.2.2. Surface Modification of AC

Aliquot of the AC was aminated, as shown in Figure 2. In brief, about 20 g of the precleaned and dried bamboo stock material was outgassed under nitrogen gas fed at 100 $mL \cdot min^{-1}$ in an electric tubular furnace, ramped at 10 $°C \cdot min^{-1}$ to 800 °C. Upon reaching the target temperature, the feed flow was switched to ammonia gas fed at 100 mL/min for 2 h. Afterwards, the furnace was allowed to cool to 100 °C as the gas flow was switched back to nitrogen, which flushed out residual ammonia gas as the system further cooled

to room temperature. Finally, the prepared adsorbent was retrieved and stored in an airtight electric desiccator before use [29]. All gas flows were accurately quantitated using a mass-flow controller (MFC). Samples without surface treatment were named BAC, CAC1, and CAC2, while the respective ones aminated were denoted as BAC-N, CAC1-N, and CAC2-N.

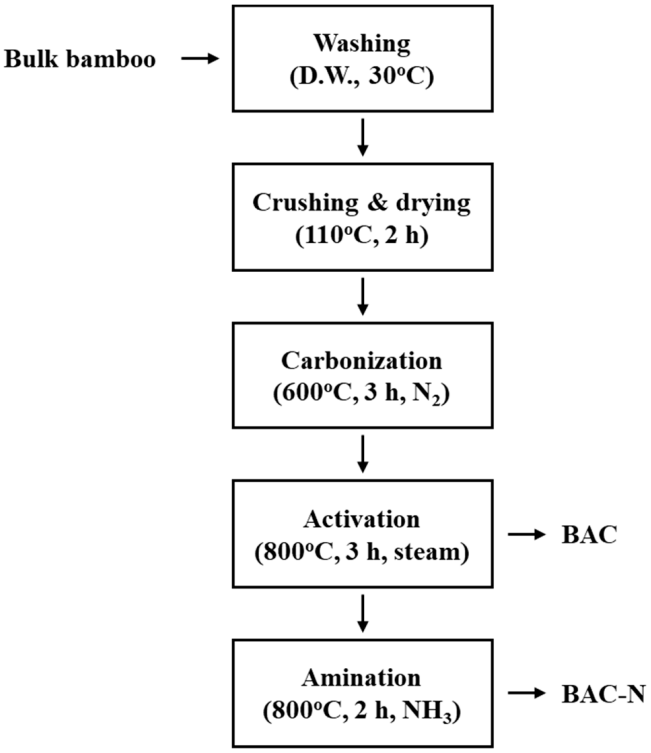

Figure 1. Scheme showing the fabrication of bamboo-based CO_2-activated carbon via amination.

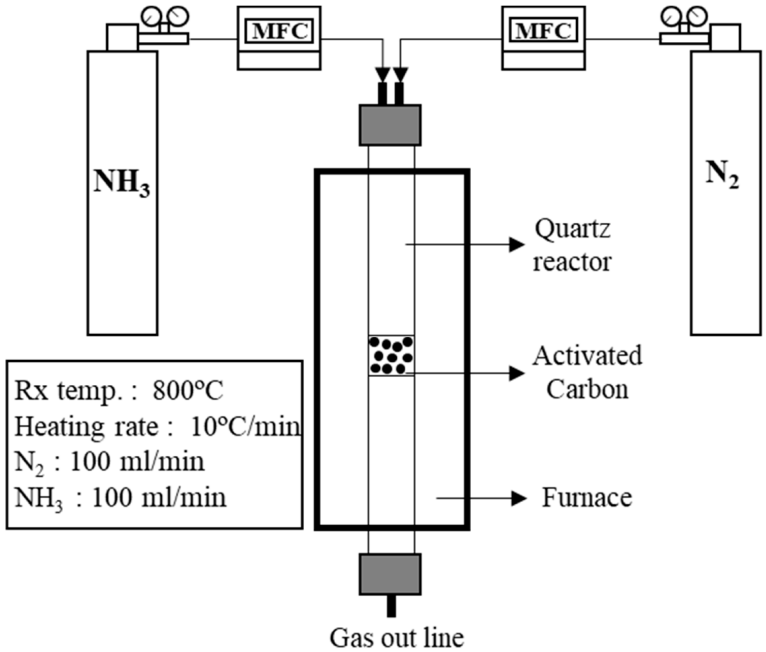

Figure 2. Schematic setup for surface amination of activated carbons. MFC: Mass-flow controller; Rx: Reaction.

2.2.3. Characterization of the Activated Carbon Adsorbents

The AC pore structure determines its maximum adsorption amount against specific gaseous pollutants, and the adsorption selectivity varies depending on the surface chemical properties [30]. A BET device (Belsorp-mini, Microtrac BEL, Tokyo, Japan) determined the specific surface area and pore size distribution at 77 K. The MP plot analysis closely evaluated the distribution of micropores favorable for CO_2 adsorption. Before the analysis, the samples were outgassed under an N_2 atmosphere at 110 °C for 6 h to maintain their intrinsic state.

The chemical properties of the ACs were quantitively investigated using the XRF technique (X-ray Fluorescence Spectroscopy; Rigaku, Japan) to obtain the relative non-CHNO (metallic) composition. Further ultimate analysis was carried out (using Flash 1112(CE) Thermo Fisher Scientific Inc., Branchburg, NJ, USA) on BAC and BAC-N samples to investigate the influence of amination on the CHNO composition and eventual CO_2 adsorption. The analysis was performed at 1000 °C on approximately 5 mg of the test samples under N_2 atmosphere, fed at 100 mL·min^{-1}. The %CHN compositions were determined from the gas vent while %O makes it up to 100%, following the Equation (1):

$$C_aH_bN_cO_d + (a + \frac{b}{4} - \frac{d}{2})O_2 \rightarrow aCO_2 + \frac{b}{2}H_2O + \frac{C}{2}N_2 \quad (1)$$

More specifically, the nitrogen functionalities formed by the surface amination were determined by XPS (X-ray Photoelectron Spectroscopy; K-Alpha, Thermo Fisher Scientific Inc., Branchburg, NJ, USA). Here, the XPS spectra were obtained with a Thermo-electron photoelectron spectrometer using monochromatized Al K-α radiation (1486.6 eV), with the source at 15 kV and 34 mA. The survey scans were collected from 0 to 1200 eV with a pass energy of 50 eV. The N 1s high-resolution scans were performed over 410–395 eV. The measurement was calibrated based on the C 1s bond corresponding to graphitic carbon at 284.6 eV. After subtracting the baseline, the curve-fitting was performed using the non-linear least-squares algorithm, assuming a Gaussian peak shape. Further, the morphology and surface elements were observed using an FE-SEM (Field Emission Scanning Electron Microscope; LEO SUPRA 55, Hamburg, Germany).

2.2.4. CO_2 Adsorption Test

The ambient low-concentration CO_2 adsorption setup is schematically depicted in Figure 3. It contains a stainless-steel tubular packed bed reactor with a diameter and height of 2.5 and 15 cm, respectively [27,28]. Approximately 3–4 g of each sorbent was used to evaluate the CO_2 amount captured. Here, we chose 3000 ppm CO_2 as our test concentration because it is the average value (i.e., 2000–4000 ppm) whereby acute health hazards (such as inflammation) could ensue [7]. Briefly, an MFC for N_2 and CO_2 quantitated the amount of each gas needed to reach a gas mixer, which ensured homogenous mixing of the feed gas that mimicked indoor air. The CO_2 concentration at the reactor outlet was measured in real time using a non-dispersive infrared sensor (CO_2 engine K30, Esense air, Delsbo, Sweden. The sensor's CO_2 measurement range is 0–5000 ppm (±30 ppm accuracy), operating at 12 V and measuring at 0.5 Hz with a response time of 20 s diffusion time. The adsorption amount was evaluated using Equation (2) from the breakthrough curve for the continuous flow [31].

$$q = \frac{QC_i}{m}\left(\int_0^t (1 - \frac{C_o}{C_i})dt\right) \quad (2)$$

Here, q is the adsorption amount (mmol·g^{-1}) of CO_2 per unit weight of adsorbent, Q is the inlet gas flow rate (cm^3·s^{-1}), C_0 and C_i are the inlet and outlet CO_2 concentrations (%), respectively, m indicates the mass of adsorbent (g), and t is the adsorption duration (min) [32].

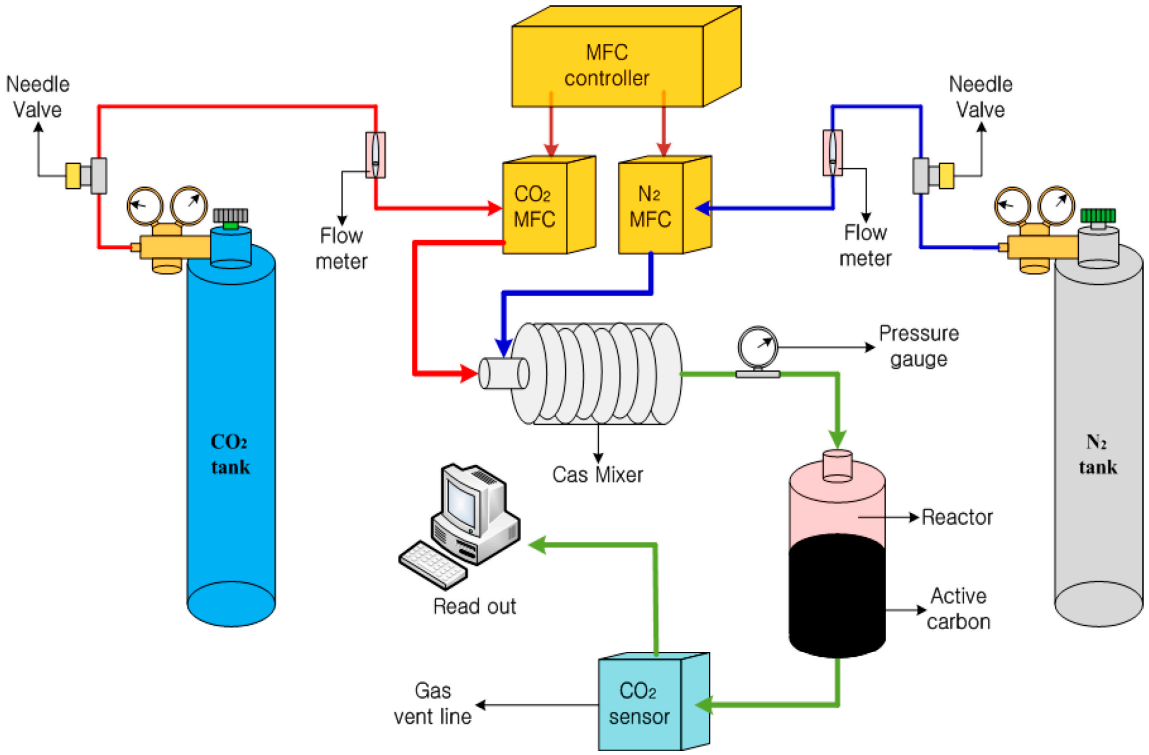

Figure 3. Schematic diagram of the ambient low-level CO_2 adsorption test setup.

Further, we investigated the sorbents' selectivity (i.e., the preferential adsorption) toward CO_2 in a binary mixture with N_2. Selectivity ($\alpha_{s,g}$) represents the ability of the adsorbent (s) to remove a fluid sorptive (g, if gaseous) under ambient condition. In this case, the selectivity of CO_2 is the ratio of the mole fractions of CO_2 retained by the sorbents to that unadsorbed, as expressed in Equations (3)–(5) [33].

$$\text{Selectivity } (\alpha_{s,g}) = \left({}^{CO_2}/_{M}\right)s \div \left({}^{CO_2}/_{M}\right)g \quad (3)$$

$$\text{i.e.,} = \sum_{t_o}^{t_b}\left(1 - {}^{C_{t_b}}/_{C_o}\right) \div \sum_{t_o}^{t_b}\left({}^{C_{t_b}}/_{C_o}\right) \quad (4)$$

$$= \sum_{t_o}^{t_b}\left({}^{C_o - C_{t_b}}/_{C_o}\right) \quad (5)$$

where M represents the matrix, and C_o and C_{t_b} are initial and breakthrough CO_2 concentrations, respectively. An $\alpha_{s,g} > 1$ implies favorable selectivity, and vice versa. The higher the value, the greater the feasibility and ease of selective adsorption [33]. Several parameters of the constituent gases, such as kinetic diameters and electric properties, driven by the pore structure and surface chemistry, influence such separations [32,34].

Then, a selectivity rate constant k_s (min^{-1}) was estimated by calculating the average amount of selectively adsorbed CO_2 before the breakthrough by dividing Equation (6) with the breakthrough time, t_b.

$$\text{Selectivity rate constant } k_s\ (min^{-1}) = \sum_{t_o}^{t_b}\left({}^{C_o - C_{t_b}}/_{C_o}\right) \div t_b. \quad (6)$$

3. Results

3.1. Preparing the AC Adsorbents

High-temperature amination impregnated basic amine functionalities on the ACs [29]. By placing the AC granules under ammonia flow in a hot tubular furnace, nitrogen functional groups from the decomposed ammonia could be impregnated on the granules.

The yield of the obtained ACs was estimated by comparing the original weight (M_i) of the raw material (that went through the washing and drying process) with the weight (M_f) of the AC obtained from the final activation step as defined in Equation (7) [32–36]. The final yields were 12–17% on a dry basis, similar to a biomass-based activated carbon prepared through chemical activation with KOH or K_2CO_3.

$$\text{Yield } (\%) = \frac{M_f}{M_i} \times 100 \quad (7)$$

3.1.1. Morphology

Figure 4 depicts the SEM micrographs of the procured coconut shell-based and the fabricated bamboo-based ACs. The bamboo-based ACs formed a regular rhombic honeycomb structure, while the coconut-based ACs exhibited irregular amorphous surface and pore structure. During carbonization, the textural characteristics are usually influenced by the distribution, location, decomposition temperature, and amount of lignin and cellulose [34,35]. Pores are formed in the granules as these substances disappear into solid carbonized substances as vapor, aerosol, and CO_2 during heat treatment [37–39]. Thus, optimum heat treatment programs to induce the decomposition of these components to form micropores have been emphasized [40].

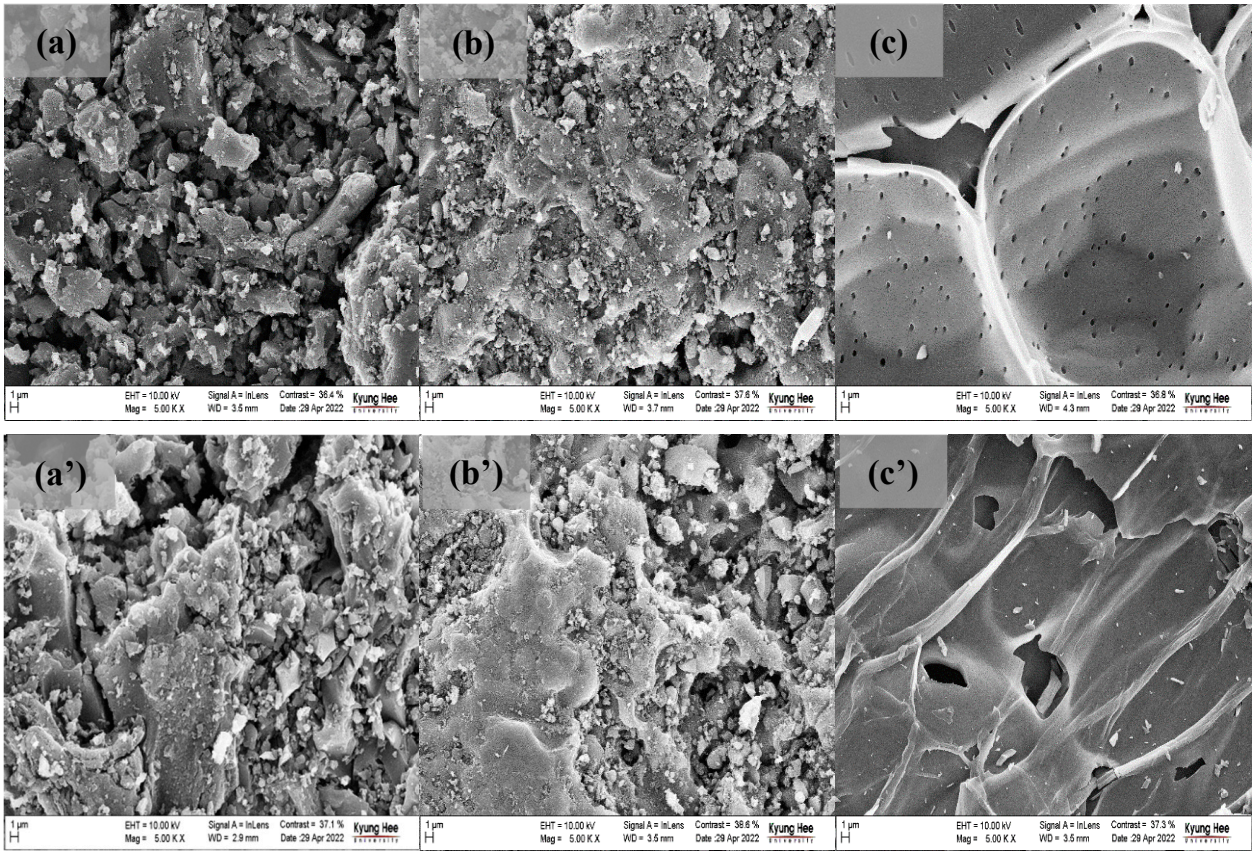

Figure 4. The SEM micrographs of (**a**) CAC1, (**a′**) CAC1-N, (**b**) CAC2, (**b′**) CAC2-N, (**c**) BAC, (**c′**) BAC-N.

3.1.2. Textural Analysis

Table 2 summarizes the BET analysis results of the samples' textural properties. The specific surface area (S_{BET}) of CAC1 and CAC2 were 1247 and 1336 $m^2 \cdot g^{-1}$, respectively, larger than that of BAC (984 $m^2 \cdot g^{-1}$). However, we found that amination improved the

S_{BET} by 8.9, 1.1, and 19.4% for CAC1-N, CAC2-N, and BAC-N, respectively, showing a much significant increase with BAC-N.

Table 2. Textural properties of BAC and coconut-based activated carbons.

Sample	[a] S_{BET} ($m^2 \cdot g^{-1}$)	[b] V_p ($cm^3 \cdot g^{-1}$)	[c] D_p (nm)	[d] V_{micro} ($cm^3 \cdot g^{-1}$)	[e] D_{micro} (nm)
BAC	984	0.42	1.8	0.42	0.7
CAC1	1247	0.56	1.8	0.55	0.6
CAC2	1336	0.77	2.3	0.54	0.7
BAC-N	1175	0.51	1.7	0.51	0.7
CAC1-N	1358	0.62	1.8	0.60	0.7
CAC2-N	1351	0.77	2.3	0.57	0.8

[a] BET specific surface area; [b] Total pore volume; [c] Mean pore diameter; [d] Total micropore volume; [e] Mean micropore diameter.

Figure 5 shows the N_2 adsorption isotherms for each sample, providing information on the sorbents' pore size distribution. BAC-N exhibited a Type I adsorption isotherm, in which surface adsorption occurs significantly under <0.1 relative pressure. Thus, the adsorption showed negligible progress [41–43]. However, a hysteresis phenomenon showing an obvious difference between adsorption and desorption amounts was observed in CAC2 and CAC2-N at $P/P_0 > 0.5$. This hysteresis phenomenon occurs when the adsorbent has cylindrical mesopores.

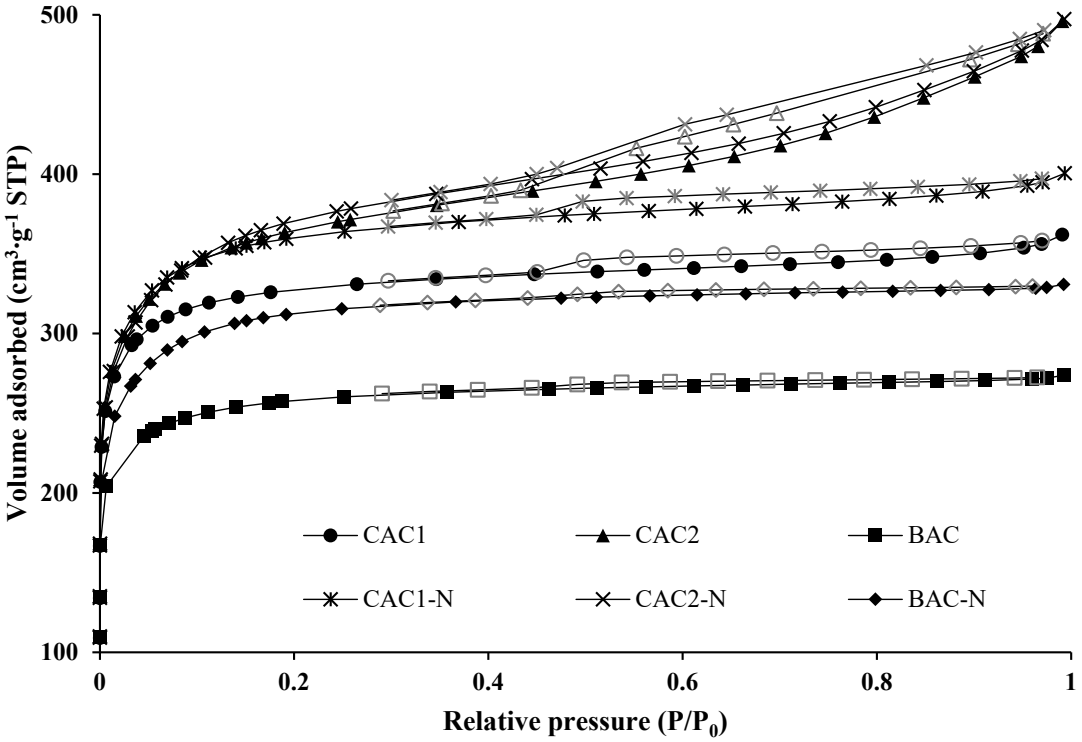

Figure 5. N_2 adsorption/desorption isotherms of the tested adsorbents at 77 K temperature. Note: Hollow and grey markers signify the desorption trends of the adsorption profiles.

Figure 6 focuses on the pore size distribution of 2 nm or fewer micropores formed in each sorbent. The graph revealed that some mesopores, in addition to micropores, were present in CAC2 and CAC2-N. Bamboo-based activated carbons with a large proportion of micropores were composed of similar pore size distributions with coconut-based samples (CAC1 and CAC1-N). Sufficient micropores facilitate CO_2 capture [44,45].

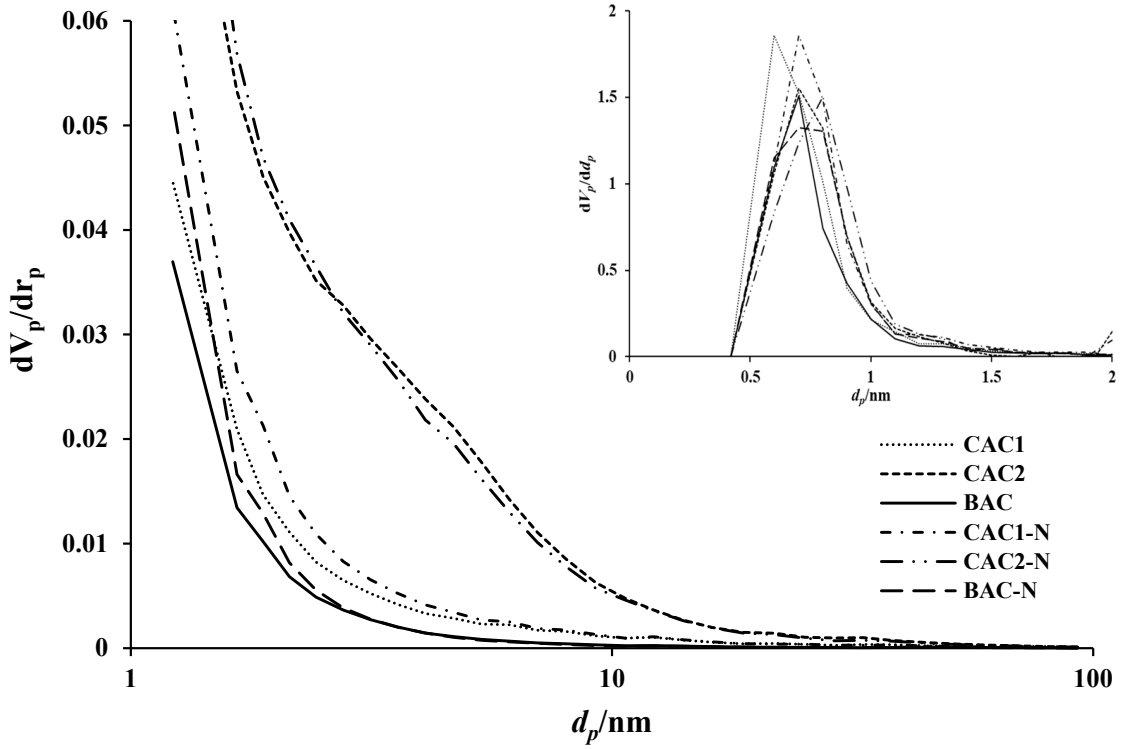

Figure 6. A BJH plot of the pore size distributions of the tested activated carbons (Insert: MP plot of the micropore size (pore diameter < 2 nm) distribution). The pore volume was auto-calculated (using MP plot equation) by the BET monosorb equipment using N_2 adsorption–desorption data.

3.2. Characterization of Chemical Structure

3.2.1. Surface Chemical Composition

Table 3 shows the elemental data of the samples before and after surface treatment as obtained from XRF and elemental analyses. Regarding the non-CHNO contents, the most abundant element in each sample was Fe at 2.42 wt% in CAC1, Cl at 3.43 wt% in CAC2, and K at 3.80 wt% in BAC. Potassium, an inorganic component that can provide basic active sites useful for CO_2 adsorption, was found to be present in the highest amount in BAC. This potassium content increased to 10.6 wt% after surface amination, estimated to be due to the relative increase in potassium as other elements decomposed or disappeared during the high-temperature chemical treatment. Moreover, the ultimate analysis confirms that CAC1 and BAC had similar N content (0.30–0.33%), about double that of CAC2 (0.14%). Upon animation, the %N of CAC1, CAC2, and BAC increased 5.6, 4.0, and 8.3 folds, respectively.

Table 3. Elemental composition of prepared activated carbons analyzed by XRF and EA.

Sample	[1] XRF Elemental Data (wt%)									[2] EA (CHNO) Elemental Data (wt%)			
	Al	Si	P	S	Cl	K	Ca	Fe	Cu	C	H	N	O
CAC1	0.097	0.785	0.304	0.568	-	1.366	1.343	2.417	-	89.2	2.03	0.33	1.56
CAC2	0.191	0.637	0.350	1.300	3.430	1.145	0.710	1.635	-	86.2	2.51	0.15	1.71
BAC	0.019	0.344	0.056	0.048	0.021	3.800	0.527	0.775	-	85.3	1.50	0.30	7.86
CAC1-N	0.131	0.870	1.931	-	-	4.810	2.875	2.233	-	81.2	1.41	1.86	2.65
CAC2-N	0.694	3.000	1.474	1.037	-	3.126	1.596	5.280	0.787	77.5	1.53	0.55	3.18
BAC-N	-	-	0.327	-	-	10.62	1.465	0.220	-	74.2	0.50	2.50	9.60

[1] X-ray fluorescence; [2] Elemental analysis.

After activation at 800 °C, additional disappearance of trace components occurred by performing surface chemical treatment again at the same temperature. As a result,

the content of other components tended to increase relatively. For example, Cu was not detected in CAC2 but appeared in trace amounts after amination (CAC2-N). Fe, a type of heavy metal substance, was simultaneously found to increase considerably. In other words, the initial sample had many acidic Cl and S components. Still, most of them disappeared as they participated in the acid–base reaction with the active species generated by ammonia decomposition. In accordance, we noticed that post-treatment with a basic gas forms alkaline active sites on the adsorbent surface and changes the chemical structure present in activated carbon.

3.2.2. Surface Functionalities

The XPS investigated the N species formed on the surface of chemically modified ACs. The N 1s XPS broad spectra were deconvoluted into various nitrogen chemical functionalities on the adsorbents (Figure 7). Detailed XPS results are supplied as Supplementary Materials. The three main N-groups identified were pyridine, pyrrole/pyridine, and quaternary nitrogen. Generally, most nitrogen functional groups are Lewis bases with a lone non-paired electron [46–48]. These weak basic functionalities form an acid–base attraction bond with CO_2, a weak Lewis acid, resulting in increased selective CO_2 removal from indoor air.

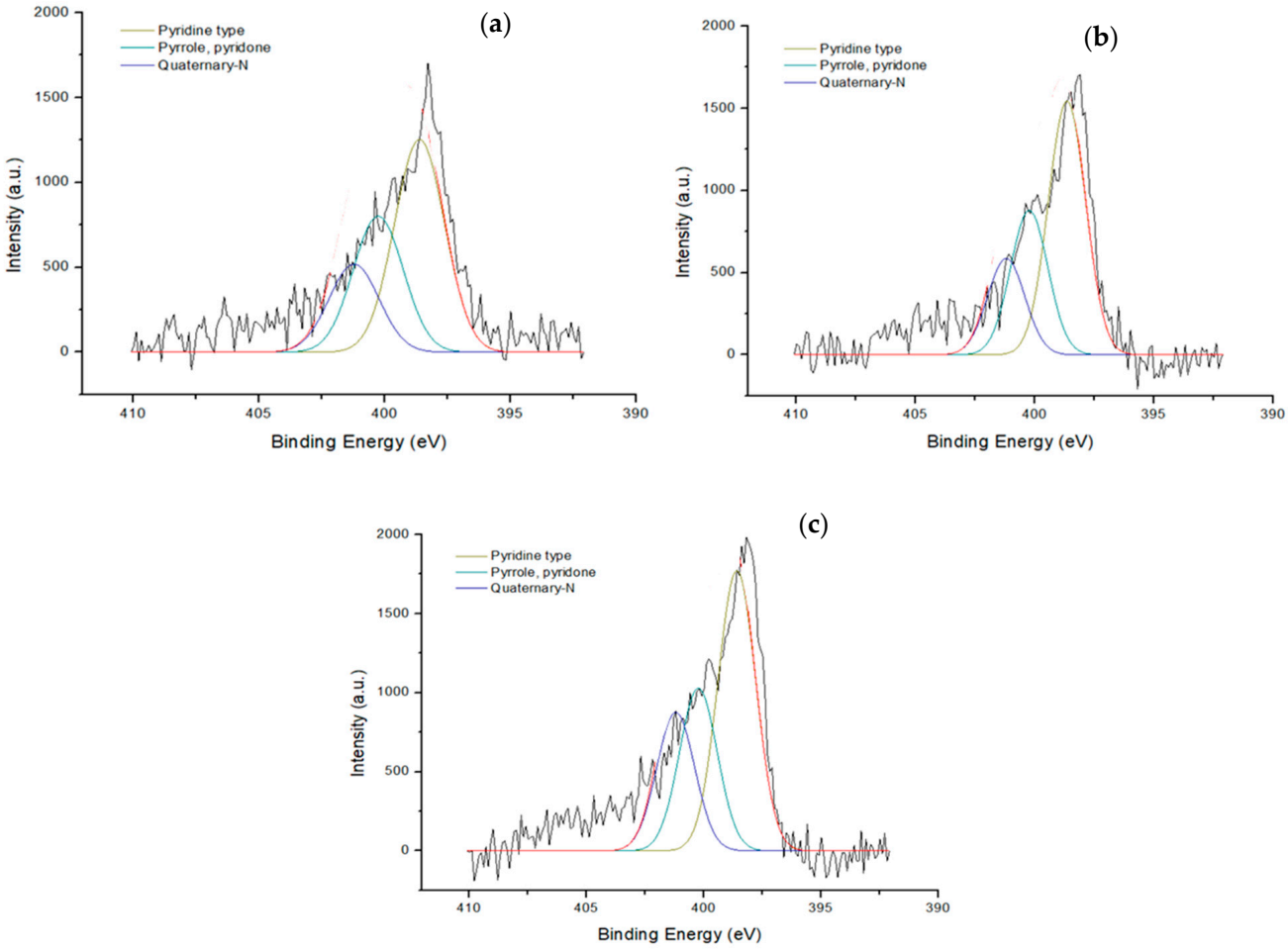

Figure 7. Deconvoluted XPS N 1s spectra of (**a**) CAC1-N, (**b**) CAC2-N, and (**c**) BAC-N. Note: The black jagged-edge and red smooth lines are the sum-raw and sum-fitted spectra, respectively.

The XPS data (Table 4) show that even under the same amination condition, the nitrogen functional groups formed on the sorbents may vary with the base carbon material used [26]. The initial BAC contained quaternary and pyrrole-dominated nitrogen compounds. However, pyridinic N was predominant in the aminated BAC (BAC-N). Research

has shown that the nitrogen functionalities often introduced on AC exhibit CO_2 preferability in the order of pyridine > quaternary > pyrrole [46]. In practice, a >30% increase in the CO_2 adsorption capacity was achieved by increasing the proportion of pyridine on an activated carbon fiber (ACF) fabricated via carbonization, activation, and amination processes of high molecular polymers [31].

Table 4. Surface nitrogen functional group of prepared activated carbons via XPS.

Sample	N-Atomic (%)	N 1s Area	Main Peak
CAC1	1.55	86.6	Quaternary
CAC2	0.61	615	Pyrrole
BAC	0.52	512	Pyrrole
CAC1-N	3.74	4108	Pyridine
CAC2-N	3.46	4311	Pyridine
BAC-N	4.33	5672	Pyridine

3.3. Evaluating the Low-Level CO_2 Adsorption Capacity

Carbon dioxide is mainly generated from occupants' breathing in indoor spaces, worsening indoor air quality and reducing comfort. National guidelines specify 1000–2000 ppm CO_2 levels depending on the facility, but it often exceeds 2000 ppm in many cases. Thus, the current study examined the effectiveness of the newly fabricated adsorbent at 3000 ppm CO_2 concentration [25,43–48]. Figure 8 shows the breakthrough curves of the 0.3% CO_2 adsorption experiment. CAC1, CAC2, BAC, CAC1-N, CAC2-N, and BAC-N achieved 6.16, 3.52, 27.29, 6.16, 5.28, and 43.13 $mg \cdot g^{-1}$ ambient 0.3% CO_2 adsorption capacity, respectively. As expected, these values are lower than the 100% CO_2 adsorption (Figure 8) at P/P_0 of 0–1.

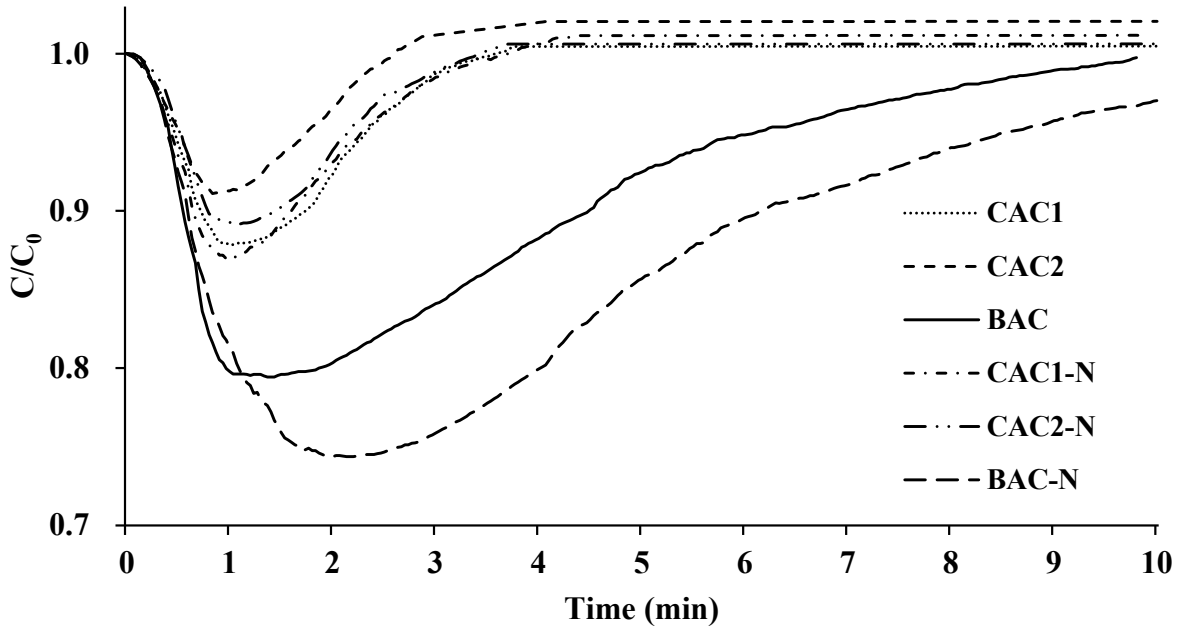

Figure 8. Breakthrough curves for the ambient adsorption of 3000 ppm CO_2 adsorption.

As shown in Figure 9, BAC and BAC-N exhibited the highest adsorption capacity of 73.9 and 79.2 $mg \cdot g^{-1}$ for pure CO_2, respectively. In contrast, CAC1-N, albeit showing relatively superior micropore volume, achieved 66.0 $mg \cdot g^{-1}$ pure CO_2 adsorption.

3.4. Evaluating the CO_2/N_2 Adsorption Selectivity

Using Equations (2)–(5), we estimated the samples' CO_2/N_2 selectivity ($\alpha_{s,g}$) and selectivity constant (Table 5).

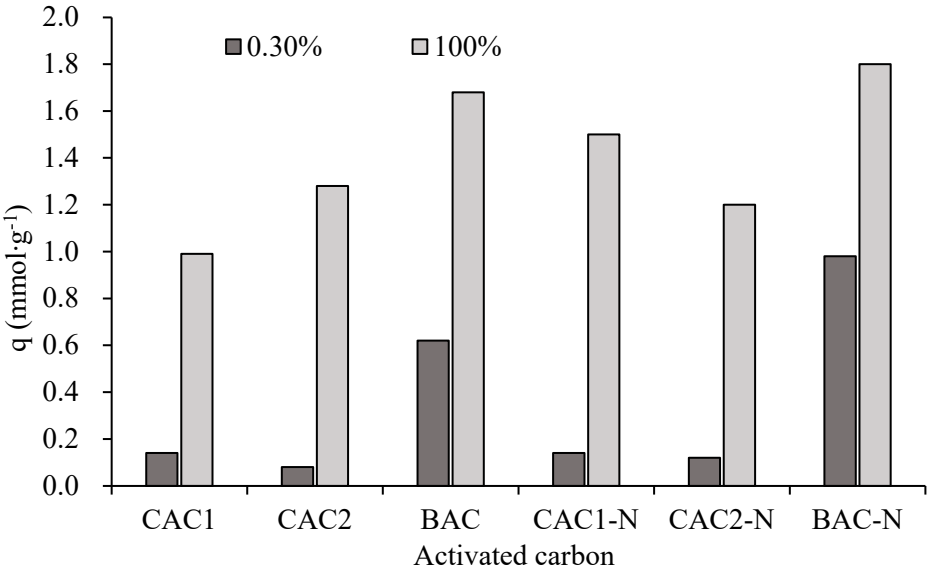

Figure 9. Comparing the adsorption capacities of the pristine, prepared, and modified activated carbon samples against indoor (0.30%) and pure (100%) CO_2 levels.

Table 5. 0.3% CO_2/N_2 selectivity and selectivity rate constant of the test adsorbents in the current study.

Sample	0.3% CO_2 q ($mmol \cdot g^{-1}$)	Breakthrough Time (t_b)	CO_2/N_2 ($\alpha_{s,g}$)	Selectivity Rate Constant k_s (min^{-1})
CAC1	0.14	3.66	1.52	5.15
CAC2	0.08	2.93	1.16	4.70
BAC	0.62	10.7	8.60	8.48
CAC1-N	0.14	3.64	1.50	5.10
CAC2-N	0.12	3.63	1.38	5.05
BAC-N	0.98	12.7	13.4	18.2

Table 5 shows that amination significantly improved the selective removal of BAC (as BAC-N) CO_2 from the binary mixture, unlike the commercial samples. We attribute the significant superior CO_2 selective adsorption by the newly fabricated adsorbents to the high potassium content of bamboo biomass [26]. The enhanced selectivity is also reflected in the selectivity constant. The improved van der Waal's force induced by the amine groups in attaching CO_2 onto the adsorbent's surface extends the breakthrough time, notably for each carbon type used in the current study.

4. Discussion

The optimal process of capturing gaseous pollutants in multi-use facilities' indoor environments is to use a dry adsorbent because of the aforementioned inherent merits of the technology [12]. Despite the textural excellence of coconut-based ACs, alternative materials are necessary due to their limited supply. In this study, we attempted to develop an adsorbent suitable for low-concentration CO_2 capture by utilizing domestic bamboo's physical and chemical properties.

Many micropores were formed in adsorbent granules as solid carbonized substances, vapor, aerosol, and CO_2 disappeared during the high-temperature manufacturing process. The increase in specific surface area after amination could be attributed to the new micropores formed or restructured accompanying the disappearing residual impurities, such as organics, due to additional reactions with the potassium component [32]. The micropore volume, as estimated by the MP plot, increased particularly for BAC, from 0.42 to 0.51 g/cm^3, while the relative pore volume increased by 97%, 74%, and 100% for

CAC1-N, CAC2-N, and BAC-N, respectively. The enhanced micropore development is expected to improve the selectivity for CO_2 [42]. Thus, optimum heat treatment programs have been emphasized to induce the decomposition of the inherent components to form micropores [43]. This study also highlighted a previous deduction that the proportion of ultramicropores is more relevant to low-level CO_2 adsorption than the total pore size, micropore size, or specific surface area [27,36].

During amination, gaseous ammonia molecules are decomposed into radicals and deposited on the surface of activated carbon, forming alkali functional groups [44]. A previous study has ensured that the alkaline active sites improve the affinity for weak acidic CO_2 molecules, leading to selective adsorption [45]. Nitrogen species were more populated on BAC-N than other samples. This occurrence is probably attributed to the abundant alkaline potassium content in bamboo. The potassium forms open spaces and physical defects on the adsorbent surface by combining with the carbonization and activation of various substances, providing conditions for widespread impregnation of amine functionalities [46]. The potassium component of interest in this study was more abundant in BAC-N, and surface amination (BAC-N) increased relative to the potassium content. However, contrary to a previous report [46], quaternary N (i.e., a nitrogen atom that has substituted a carbon atom in the graphene layer), which was deemed incapable of attracting a Lewis acid (such as CO_2) (due to the used lone pair of electrons in a dative covalent bonding) was surplus in BAC-N, which, in turn, exhibits excellent CO_2 selective adsorption. The reason for such high quaternary nitrogen could be ascribed to the high content of intrinsic potassium in the bulk of the starting material, unlike those formerly reported where external doping was carried out [2]. Thus, more N functionalities were doped into the sorbent's basal plane, leading to a high yield of quaternary nitrogen.

Compared with similar indoor CO_2 studies (Table 6), we observed that only wet impregnation with KOH stabilization with amination [28] performed better than other samples. Also, pre-oxidation to increase the active surface for tethering amine radicals during amination did not sufficiently achieve the desired results, probably because the predominant oxygen radicals (basic ones, such as carbonyl and phenolic oxygen functionalities) on the pristine and pre-oxidized carbons were refractory to desorption [47].

Table 6. Comparison of indoor CO_2 adsorption data from the literature with the current study.

S/N	Adsorbent	Fabrication/Modification Method	q (mmol·g^{-1})	Ref.
1	Coconut shell-based [1] AC	• KOH stabilization via amination	2.230	[26]
		• Wet impregnation of Ca + amination	0.280	[43]
		• Wet impregnation of Ca	0.310	[43]
		• Simple dry-phase amination	0.410	[45]
		• [2] UV-C + O_3 pre-oxidation before amination	0.260	[47]
2	Rice husk-based AC	• KOH-impregnated AC	2.100	[48]
3	Zeolite	• Cation exchanged zeolites 13	1.87	[45]
4	Bamboo-based AC	• Simple amination	0.980	[3] C.S.

[1] Activated carbon; [2] Ultravilet radaition-C; [3] Current study.

The adsorption test for pure CO_2 flow at ambient temperature and pressure was intended to estimate the maximum capture capability of the prepared adsorbents. The adsorbed CO_2 amount differed between samples based on their respective physical (specific surface area and micropore size distribution) and chemical (surface potassium concentration and nitrogen functional group nature and content) properties [49–51]. According to a relevant study, in a case of potassium-doped activated carbon, CO_2 desorption occurred at 94–117, 423–457, and 828–900 °C, whereas N-doped AC showed an additional desorption temperature range at 593–619 °C [51–53]. These assertions prove that potassium and nitrogen groups provide different active sites for CO_2 adsorption. Consequently, addi-

tional active sites originating from inherent potassium in the bamboo material enhanced the adsorption.

Our results, therefore, suggest that potassium-rich stock materials (such as bamboo, plantain peel, stem, cocoa pods, etc.) could suffice as the best starting material for developing a selective activated carbon-based low-level CO_2 adsorbent [52,53]. However, the sustainability of IAQ requires more studies on the impact of inhaled CO_2 on human health, especially in the absence of other indoor air pollutants. Such examinations have been carried out with various indoor CO_2 levels, e.g., 5000 ppm [54], 800–3000 ppm [55], 830 and 27,000 [56], 1450 ppm [57], 8000–12,000 [58], 6000–2100 ppm [59], 900 ppm [60], etc.

5. Conclusions

To circumvent the high energy demand associated with maintaining normal indoor CO_2 levels via ventilation, this study fabricated a lignocellulosic adsorbent from abundantly available local bamboo trees for selective capture of CO_2. The bamboo specimen was carbonized, steam activated, and then aminated to increase the active sites. The specific surface area and pore volume of the activated adsorbent were 984 $m^2 \cdot g^{-1}$ and 0.42 $cm^3 \cdot g^{-1}$, respectively. They were, however, improved to 1175 $m^2 \cdot g^{-1}$ and 0.53 $cm^3 \cdot g^{-1}$ by high-temperature amination. The obtained sample, BAC-N, showed 0.98 mmol/g (43.13 $mg \cdot g^{-1}$) of adsorption amount for 3000 ppm CO_2, higher than the coconut-based commercial activated carbons. In particular, amine groups doped on the adsorbent enhanced the potential of the inherent potassium in the bamboo raw material for selective CO_2 adsorption. Consequently, as an alternative to the laborious and energy-intensive methods commonly used to maintain a conducive and healthy indoor air, this study offers a sustainable approach for fabricating a reliable, available, and affordable dry scrubbing method.

Further research to improve the sustainability of the process should attempt to reduce the energy requirement for the amination and also carry out regeneration tests on the adsorbent. Also, the amination of other potassium-rich materials (such as plantain peel or stem and cocoa pods) should be compared with the results from the current study and those from potassium-modified activated carbon to confirm the influence of quaternary nitrogen in selective CO_2 adsorption. In addition, the regeneration (recycle and reuse), adsorption isotherm, kinetics, and thermodynamics should be conducted to model its real-life applicability and sustainability accurately and conclusively.

Supplementary Materials: The following supporting information can be downloaded at: https://www.mdpi.com/article/10.3390/su16041634/s1.

Author Contributions: Conceptualization, Y.J.; Methodology, W.K.; Validation, A.A.A.; Investigation, S.H. and W.K.; Writing—original draft, S.H.; Writing—review & editing, Y.J. and A.A.A.; Visualization, S.H. and A.A.A.; Supervision, W.K. and Y.J.; Funding acquisition, Y.J. All authors have read and agreed to the published version of the manuscript.

Funding: This research acknowledges the support from the National Research Foundation of Korea grant (2022R1F1A106547711).

Institutional Review Board Statement: Not applicable.

Informed Consent Statement: Not applicable.

Data Availability Statement: Data are contained within the article and supplementary materials.

Conflicts of Interest: The authors declare no conflict of interest.

References

1. Karimi, H.; Adibhesami, M.A.; Bazzazzadah, H.; Movafagh, S. Green buildings: Human-centered and energy efficiency optimization strategy. *Energies* **2023**, *16*, 3681. [CrossRef]
2. Mannan, M.; Al-Ghamdi, S.G. Indoor air quality in buildings: A comprehensive review on the factors influencing air pollution in residential and commercial structure. *Int. J. Environ. Res. Public Health* **2021**, *18*, 3276. [CrossRef]

3. Burridge, H.C.; Bhagat, R.K.; Stettler, M.E.J.; Kumar, P.; De Mel, I.; Demis, P.; Hart, A.; Johnson-Llambias, Y.; King, M.F.; Klymenko, O.; et al. The ventilation of buildings and other mitigating measures for COVID-19: A focus on wintertime. *Proc. R. Soc. A* **2021**, *477*, 20200855. [CrossRef]
4. Moreno-Rangel, A.; Sharpe, T.; Musau, F.; McGill, G. Field evaluation of a low-cost indoor air quality monitor to quantify exposure to pollutants in residential environments. *J. Sens. Sens. Syst.* **2018**, *7*, 373. [CrossRef]
5. Kumar, P.; Hama, S.; Abbass, R.A.; Nogueira, T.; Brand, V.S.; Wu, H.-W. CO_2 exposure, ventilation, thermal comfort and health risks in low-income home kitchens of twelve global cities. *J. Build. Eng.* **2022**, *61*, 105254. [CrossRef]
6. Gawande, S.; Tiwari, R.R.; Narayanan, P.; Bhadri, A. Indoor air quality and sick building syndrome: Are green buildings better than conventional buildings? *Indian J. Occup. Environ. Med.* **2020**, *24*, 30–32.
7. Jacobson, T.A.; Kler, J.S.; Hernke, M.T.; Braun, R.K.; Meyer, K.C.; Funk, W.E. Direct human health risks of increased atmospheric carbon dioxide. *Nat. Sustain.* **2019**, *2*, 691–701. [CrossRef]
8. Lowther, S.D.; Dimitroulopoulou, S.; Foxall, K.; Shrubsole, C.; Cheek, E.; Gadeberg, E.; Sepai, O. Low level carbon dioxide indoor–A pollution indicator or a pollutant? A health-based perspective. *Environments* **2021**, *8*, 125. [CrossRef]
9. Lee, M.; Ham, J.; Lee, J.-W.; Cho, H. Analysis of thermal comfort, energy consumption, and CO_2 reduction of indoor space according to the type of local heating under winter rest conditions. *Energy* **2023**, *268*, 126722. [CrossRef]
10. Hattori, S.; Iwamatsu, T.; Miura, T.; Tsutsumi, F.; Tanaka, N. Investigation of indoor air quality in residential buildings by measuring CO_2 concentration and a questionnaire survey. *Sensors* **2022**, *22*, 7331. [CrossRef]
11. Raupach, M.R.; Davis, S.J.; Peters, G.P.; Andrew, R.M.; Canadell, J.G.; Ciais, P.; Le Quere, C. Sharing a quota on cumulative carbon emissions. *Nat. Clim. Chang.* **2014**, *4*, 873–879. [CrossRef]
12. Huston, N.D. Structural effects on the high-temperature adsorption of CO_2 on a synthetic hydrotalcite. *Chem. Mater.* **2004**, *16*, 4135–4143. [CrossRef]
13. Kim, Y.E.; Choi, J.H.; Yun, S.H.; Nam, S.C.; Yoon, Y.I. CO_2 capture using aqueous solution of K_2CO_3-methylpiperazine and monoethanolamine: Specific heat capacity and heat of absorption. *Korean J. Chem. Eng.* **2016**, *33*, 3465–3472. [CrossRef]
14. Pintola, T.; Tontiwachwuthikul, P.; Meisen, A. Simulation of pilot plant and industrial CO_2 MEA absorbers. *Gas Sep. Purif.* **1993**, *7*, 47–52. [CrossRef]
15. Strazisar, B.R. Degradation pathways for monoethanolamine in a CO_2 capture facility. *Energy Fuels* **2003**, *17*, 1034–1039. [CrossRef]
16. Herzog, H. *An Introduction to CO_2 Separation and Capture Technologies*; Massachusetts Institute of Technology: Cambridge, MA, USA, 1999; pp. 1–8.
17. Rougerol, F.; Rougerol, J.; Sing, K. *Adsorption by Powders and Porous Solids*; Academic Press: London, UK, 2012. [CrossRef]
18. Gamal, M.; Mousa, H.A. Bio regeneration of activated carbon: A comprehensive review. Fuel Processing Technology. *Sep. Purif. Technol.* **2018**, *197*, 345–359. [CrossRef]
19. Bai, J.; Huang, J.; Yu, Q.; Demir, M.; Akgul, E.; Altay, B.N.; Hu, X.; Wang, L. Fabrication of coconut shell-derived porous carbons for CO_2 adsorption application. *Front. Chem. Sci. Eng.* **2023**, *17*, 1122–1130. [CrossRef]
20. Duan, C.; Meng, M.; Huang, H.; Wang, H. Performance and characterization of bamboo-based activated carbon prepared by boric acid activation. *Mater. Chem. Phys.* **2023**, *295*, 127130. [CrossRef]
21. Sarkisov, L. Accessible surface area of porous materials: Understanding theoretical limits. *Adv. Mater.* **2012**, *24*, 3130–3133. [CrossRef]
22. Park, J.-W.; Ly, H.V.; Oh, C.; Kim, S.-S. Preparation and characterization of bamboo-based activated carbon by phosphoric acid and steam activation. *Clean Technol.* **2019**, *25*, 129–139. [CrossRef]
23. Shao, Y.; Li, J.; Fang, X.; Yang, Z. Chemical modification of bamboo activated carbon surface and its adsorption property of simultaneous removal of phosphate and nitrate. *Chemosphere* **2022**, *287*, 132118. [CrossRef]
24. Li, S.; Zhou, S.; Zhao, G. Tuning the morphology of micro and nanospheres from bamboo shoot shell cytosol lignin. *Ind. Corps Prod.* **2021**, *171*, 113860. [CrossRef]
25. Wei, H.; Deng, S.; Hu, B.; Chen, Z.; Wang, B.; Huang, J.; Yu, G. Granular bamboo-derived activated carbon for high CO_2 adsorption: The dominant role of narrow micropores. *ChemSusChem* **2012**, *5*, 2354–2360. [CrossRef]
26. Wu, W.; Wu, C.; Zhang, G.; Liu, J.; Li, Y.; Li, G. Synthesis and characterization of magnetic K_2CO_3-activated carbon produced from bamboo shoot for the adsorption of Rhodamine b and CO_2 capture. *Fuel* **2023**, *332*, 126107. [CrossRef]
27. Adelodun, A.A.; Lim, Y.H.; Jo, Y.M. Stabilization of potassium-doped activated carbon by amination for improved CO_2 selective capture. *J. Anal. Appl. Pyrolysis* **2014**, *108*, 151–159. [CrossRef]
28. Babinszki, B.; Sebestyén, Z.; Jakab, E.; Kőhalmi, L.; Bozi, J.; Várhegyi, G.; Wang, L.; Skreiberg, Ø.; Czégény, Z. Effect of slow pyrolysis conditions on biocarbon yield and properties: Characterization of the volatiles. *Bioresour. Technol.* **2021**, *338*, 125567. [CrossRef]
29. Laine, J.; Yunes, S. Effect of the preparation method on the pore size distribution of activated carbon from coconut shell. *Carbon* **1992**, *30*, 601–604. [CrossRef]
30. Goel, C.; Dinesha, S. CO_2 capture by adsorption on biomass-derived activated char: A review. *Sci. Total Environ.* **2021**, *798*, 149296. [CrossRef]
31. Mochizuki, Y.; Bud, J.; Byambajav, E.; Tsubouchi, N. Influence of ammonia treatment on the CO_2 adsorption of activated carbon. *J. Environ. Chem. Eng.* **2022**, *10*, 107273. [CrossRef]

32. El-Nemr, M.; El Nemr, A.; Hassaan, M.A.; Ragab, S.; Tedone, L.; De Mastro, G.; Pantaleo, A. Microporous activated carbon from *Pisum sativum* pods using various activated methods and tested for adsorption of acid orange 7 dye from water. *Molecules* **2022**, *27*, 4840. [CrossRef]
33. Kim, T.K.; Suh, M.P. Selective CO_2 adsorption in a flexible non-interpenetrated metal-organic framework. *Chem. Commun.* **2011**, *14*, 4258–4260. [CrossRef] [PubMed]
34. Correa, C.R.; Otto, T.; Kruse, A. Influence of the biomass components on the pore formation of activated carbon. *Biomass Bioenergy* **2016**, *97*, 53–64. [CrossRef]
35. Araujo, T.; Parnell, A.J.; Bernardo, G.; Mendes, A. Cellulose-based carbon membranes for gas separations—Unravelling structural parameters and surface chemistry for superior separation performance. *Carbon* **2023**, *204*, 398–410. [CrossRef]
36. Altintig, E.; Sarici, B.; Karataş, S. Prepared activated carbon from hazelnut shell where coated nanocomposite with Ag^+, used for antibacterial and adsorption properties. *Emviron. Sci. Pollut. Res. Int.* **2022**, *30*, 13671–13687. [CrossRef]
37. Patawat, C.; Silakate, K.; Chuan-Udom, S.; Supanchaiyamat, N.; Hunt, A.J.; Ngernyen, Y. Preparation of activated carbon from Dipterocarpus alatus fruit and its application for methylene blue adsorption. *RSC Adv.* **2020**, *36*, 21082. [CrossRef] [PubMed]
38. Tay, T.; Ucar, S.; Karagoz, S. Preparation and characterization of activated carbon from waste biomass. *J. Hazard. Mater.* **2009**, *165*, 481–485. [CrossRef]
39. Zuo, S.-L.; Gao, S.-Y.; Yuan, X.-G.; Xu, B.-S. Carbonization mechanism of bamboo (Phyllostachys) by means of Fourier Transform Infrared and elemental analysis. *J. For. Res.* **2003**, *14*, 75–79. [CrossRef]
40. Zhu, Y.; Huang, J.; Wang, K.; Wang, B.; Sun, S.; Lin, X.; Song, L.; Wu, A.; Li, H. Characterization of Lignin Structures in Phyllostachys edulis (Moso Bamboo) at Different Ages. *Polymers* **2020**, *12*, 187. [CrossRef]
41. Czernik, C.; Bridgwater, V. Overview of applications of biomass fast pyrolysis oil. *Energy Fuels* **2006**, *18*, 590–598. [CrossRef]
42. Zhang, D.; Wei, W.; Lu, L.; Jin, H.; Guo, L. Variation of pore structure in Zhundong coal particle with stepped K_2CO_3 loading during supercritical water gasification. *Fuel* **2021**, *305*, 121457. [CrossRef]
43. Adelodun, A.A.; Jo, Y.M. Integrated basic treatment of activated carbon for enhanced CO_2 selectivity. *Appl. Surf. Sci.* **2013**, *286*, 306–313. [CrossRef]
44. Bai, J.; Huang, J.; Yu, Q.; Demir, M.; Kilic, M.; Altay, B.N.; Hu, X.; Wang, L. N-doped porous carbon derived from macadamia nut shell for CO_2 adsorption. *Fuel Process. Technol.* **2023**, *249*, 107854. [CrossRef]
45. Lee, K.-M.; Lim, Y.-H.; Park, C.-J.; Jo, Y.-M. Adsorption of low-level CO_2 using modified zeolites and activated carbon. *Ind. Eng. Chem. Res.* **2012**, *51*, 1355–1363. [CrossRef]
46. Jo, Y.-M.; Hong, H.-E.; Adelodun, A.A. Preparation of KOH impregnated AC pellets for selective CO_2 capture. *J. Korean Soc. Odor Res. Eng.* **2013**, *12*, 203–209.
47. Adelodun, A.A.; Lim, Y.-H.; Jo, Y.-M. Effect of UV-C on pre-oxidation prior amination for preparation of a selective CO_2 adsorbent. *J. Anal. Appl. Pyrolysis* **2014**, *105*, 191–198. [CrossRef]
48. Wang, S.; Lee, Y.-R.; Won, Y.; Kim, H.; Jeong, S.-E.; Hwang, B.W.; Cho, A.R.; Kim, J.-Y.; Park, Y.C.; Nam, H.; et al. Development of high-performance adsorbent using KOH-impregnated rice husk-based activated carbon for indoor CO_2 adsorption. *Chem. Eng. J.* **2022**, *437*, 135378. [CrossRef]
49. Sevilla, M.; Fuertes, A.B. CO_2 adsorption by activated templated carbons. *J. Colloid Interface Sci.* **2012**, *366*, 147–154. [CrossRef]
50. Swietlik, U.; Grzyb, B.; Torchala, K.; Gryglewicz, G.; Machnikowski, J. High-temperature ammonia treatment of pitch particulates and fibers for nitro-gen enriched microporous carbons. *Fuel Process. Technol.* **2014**, *119*, 211–217. [CrossRef]
51. Dilokekunakul, W.; Teerachawanwong, P.; Klomkliang, N.; Supasitmongkol, S.; Chaemchuen, S. Effects of nitrogen and oxygen functional groups and pore width of activated carbon on carbon dioxide capture: Temperature dependence. *Chem. Eng. J.* **2020**, *389*, 124413. [CrossRef]
52. Petrovic, B.; Gorbounov, M.; Soltani, S.M. Influence of surface modification on selective CO_2 adsorption: A technical review on mechanisms and methods. *Microporous Mesoporous Mater.* **2021**, *312*, 110751. [CrossRef]
53. Hui, T.S.; Zaini, M.A.A. Potassium hydroxide activation of activated carbon: A commentary. *Carbon Lett.* **2015**, *16*, 275–280. [CrossRef]
54. Azuma, K.; Kagi, N.; Yanagi, U.; Osawa, H. Effects of low-level inhalation exposure to carbon dioxide in indoor environments: A short review on human health and psychomotor performance. *Environ. Int.* **2018**, *121*, 51–56. [CrossRef]
55. Kuga, K.; Ito, K.; Wargocki, P. The effects of warmth and CO_2 concentration, with and without bioeffluents, on the emission of CO_2 by occupants and physiological responses. *Indoor Air* **2021**, *31*, 2176–2187. [CrossRef] [PubMed]
56. Snow, S.; Boyson, A.S.; Paas, K.H.W.; Gough, H.; King, M.-F.; Barlow, J.; Noakes, C.J.; Schraefel, M.C. Exploring the physiological, neurophysiological and cognitive performance effects of elevated carbon dioxide concentrations indoors. *Build. Environ.* **2019**, *156*, 243–252. [CrossRef]
57. Mishra, A.K.; Schiavon, S.; Wargocki, P.; Tham, K.W. Respiratory performance of humans exposed to moderate levels of carbon dioxide. *Indoor Air* **2021**, *31*, 1540–1552. [CrossRef] [PubMed]
58. Tu, Z.; Geng, S.; Zhou, K.; Wang, R.; Dong, X. Human responses to high levels of carbon dioxide and air temperature. *Indoor Air* **2020**, *31*, 872–886. [CrossRef]

59. Chen, D.; Huebner, G.; Bagkeris, E.; Ucci, M.; Mumovic, D. Effects of short-term exposure to moderate pure carbon dioxide levels on cognitive performance, health symptoms and perceived indoor environment quality. *Build. Environ.* **2023**, *245*, 110967. [CrossRef]
60. Park, S.; Song, D. CO_2 concentration as an indicator of indoor ventilation performance to control airborne transmission of SARS-CoV-2. *J. Infect. Public Health* **2023**, *16*, 1037–1044. [CrossRef]